



Cite this: *Polym. Chem.*, 2018, **9**, 1206

# Synthesis of indocyanine green functionalized comblike poly(aspartic acid) derivatives for enhanced cancer cell ablation by targeting the endoplasmic reticulum†

Jiaxun Wan,<sup>a</sup> Luyan Sun,<sup>a</sup> Pan Wu,<sup>a</sup> Fang Wang,<sup>a</sup> Jia Guo,<sup>a</sup> Jianjun Cheng<sup>b</sup> and Changchun Wang<sup>b\*</sup>

Undesired gene expression can lead to severe diseases such as cancers. Oncogenic proteins or survival factors encoded by oncogenes can sustain cancer cell survival and proliferation. Considering that proteins are manufactured and transported by the endoplasmic reticulum (ER), the destroying of oncogenic proteins within the ER could cut-off the process of undesired gene expression. In this study, a new type of ER targeting strategy was developed based on the coordination interaction of the Ca(II) ion rich ER lumen with the carboxyl group of poly(aspartic acid) (PAsp). A comblike polymer PAsp-*g*-(PEG-ICG) was rationally designed and successfully prepared by grafting azido-modified polyethylene glycol (PEG) and the azido-modified photosensitizer indocyanine green (ICG) onto alkynyl-modified PAsp through the copper(I)-catalyzed alkyne-azide cycloaddition (CuAAC). Here, ICG not only shows its importance as an imaging agent that reveals the distribution of PAsp-*g*-(PEG-ICG) micelles both at tissue and subcellular levels, but also acts as a protein destructive agent to generate reactive oxygen species (ROS) resulting in protein denaturation. Moreover, chemotherapeutic drugs, such as paclitaxel, can be easily encapsulated into PAsp-*g*-(PEG-ICG) (PTX@PAsp-*g*-(PEG-ICG)) in up to 28% drug loading capacity with excellent stability. The experimental results proved that the as-prepared PTX@PAsp-*g*-(PEG-ICG) micelles exhibited selective accumulation in the ER lumen of cancer cells. Thus, a 10-fold enhancement of ROS was obtained by incubating cancer cells with PAsp-*g*-(PEG-ICG) micelles at a PTX concentration of 1.0  $\mu\text{g ml}^{-1}$  under laser irradiation (0.2  $\text{W cm}^{-2}$ , 785 nm, 30 s) for 24 h, leading to disruption of proteins in the ER that caused ER stress-induced cancer cell apoptosis up to 76%. In a cytotoxicity test, U-87 MG glioma cells incubated with PTX@PAsp-*g*-(PEG-ICG) at the PTX concentration of 2.5  $\mu\text{g ml}^{-1}$  were reduced to nearly 0% of cell viability upon 24 h laser irradiation (2  $\text{W cm}^{-2}$ , 785 nm, 30 s), in comparison with free PTX that showed 60% cell viability under the same conditions, indicating that photodynamic therapy (PDT) remarkably enhanced chemotherapeutic effects. With the good combination of PDT and chemotherapy, the PTX@PAsp-*g*-(PEG-ICG) micelles offer unprecedented advantages by effectively targeting the ER and displayed a prolonged retention time in the tumors of U-87 MG bearing nude mice, providing great promise for manipulating biomaterial design to achieve the intended ER targeted delivery for non-invasive cancer therapy.

Received 27th November 2017,  
Accepted 5th February 2018

DOI: 10.1039/c7py01994g

rsc.li/polymers

<sup>a</sup>State Key Laboratory of Molecular Engineering of Polymers and Department of Macromolecular Science, Fudan University, Shanghai 200433, P.R. China.  
E-mail: ccwang@fudan.edu.cn

<sup>b</sup>Department of Materials Science and Engineering, University of Illinois at Urbana-Champaign, Urbana, Illinois 61801, USA

†Electronic supplementary information (ESI) available. See DOI: 10.1039/c7py01994g

## Introduction

As proteins are essential for cell signalling and ligand binding,<sup>1</sup> protein biosynthesis is strictly regulated by multiple steps, including DNA transcription, RNA translation, polypeptide folding and assembling. Any error in this cascade system can lead to severe diseases, such as cancers, which is thought to be caused by activation of oncogenes.<sup>2</sup> Therefore, gene therapy represents a promising method to fundamentally rectify these errors. Along with considerable progress in the field of gene therapy, the clustered regularly interspaced short

palindromic repeat (CRISPR)/CRISPR associated protein 9 (CRISPR/Cas9) system, as a candidate prokaryote-derived genome editing tool, has made its way into a wide range of cultured cell types and organisms due to the effective genome editing and ease of usage.<sup>3,4</sup> However, the large size of Cas9 proteins still lie ahead for penetrating the cell nucleus thus limiting their efficiency in genome editing (<30%), which also may bring the safety concern as a result of off-target and delivery inefficiency to restrict their wide application in clinical trials.<sup>5,6</sup>

On the basis of the genetic information flow by DNA–RNA-proteins, information errors occurring in this cascade process have given rise to many opportunities for remediation. For example, destroyed proteins within the endoplasmic reticulum (ER) could cut-off the assembling and transportation process of oncogenic proteins or survival factors. In this regard, the development of an ER-targeted drug delivery system is required to deliver protein destruction agents. As the ER contains Ca(II) ions at a concentration up to the millimolar level, whereas the cytosolic Ca(II) concentration is ~100 nanomolar,<sup>7</sup> we hypothesized that the carboxyl-containing polymers were able to target the ER lumen through the strong coordination affinity of the Ca(II) ion to the multi-carboxyl group of the polymer. For example, the carboxyl group-containing poly(aspartic acid) (PAsp) has strong coordination affinity to Ca(II) ions, and PAsp could inhibit undissolvable CaCO<sub>3</sub> at a PAsp concentration of 4 µg ml<sup>-1</sup> with nearly 100% efficiency.<sup>8</sup> Meanwhile, PAsp is also safe in clinical applications, and a PAsp based drug delivery system is under phase III trials now.<sup>9</sup>

There are two major types of preparation methods of PAsp derivatives: (i) ring opening polymerization of *b*-benzyl-L-aspartate *N*-carboxyanhydride (NCA) with a primary amine terminated molecule under anhydrous conditions,<sup>10–12</sup> it is sophisticated and not easy to control, and (ii) the reaction of a primary amine terminated molecule, such as amine terminated PEG chains, with polysuccinimide (PSI),<sup>13–15</sup> which was inefficient at ambient temperature and an increasing reaction temperature was required to improve the reaction efficiency, but led to the degradation of PSI during the reaction.<sup>16,17</sup>

Herein, we designed and prepared a new type of biodegradable comblike polymer, poly(aspartic acid)-*graft*-(PEG-ICG) (PAsp-*g*-(PEG-ICG)), using a facile synthetic approach that could be carried out under mild conditions. As a stealth material in blood, PEG was selected to endow the nanomaterials with reduced uptake by the reticular endothelial system and prolonged blood circulation time, which is beneficial for nano-drug application.<sup>18</sup> We also chose a near-infrared photosensitizer, indocyanine green (ICG), as an imaging agent, not only owing to its excellent safety profile approved by the Food and Drug Administration (FDA) and long-time safe usage over 60 years, but also due to its lower tissue background noise and higher imaging depth.<sup>19</sup> More importantly, ICG could exhibit photodynamic therapy (PDT) and photothermal therapy (PTT) effects under near-infrared light irradiation.<sup>20</sup> As PDT has been extensively explored for

cancer treatment, under irradiation of a photosensitizer (PS) in the presence of oxygen, highly reactive oxygen species (ROS) could be generated followed by causing damage to many cellular compartments. In the ER, ROS could also cause progressive modification of proteins, leading to ER stress and eventual apoptosis of cancer cells.<sup>21,22</sup> The short lifetime of ROS in cells (approximately tens of nanoseconds) limits their diffusion depth to tens of nanometers in cells.<sup>23</sup> Thus, the photodynamic induced therapeutic effect would occur at or near the location of the PS.<sup>24</sup> For the desired use of PDT to destroy proteins within the ER, the PS therefore needs to be delivered into the ER lumen so that the generated ROS could disrupt proteins within the ER. The overwhelming ER stress would tip the balance towards cancer cell death, while the normal cells without light irradiation or PS would stay intact. Therefore, we utilized ICG to track the location of PAsp derivative micelles both *in vitro* and *in vivo*, at the same time utilizing PDT and PTT effects to destroy oncogenic proteins or survival factors within the ER. Chemotherapeutic agents such as paclitaxel could be easily encapsulated by PAsp-*g*-(PEG-ICG) (PTX@PAsp-*g*-(PEG-ICG)) with high loading content. By integrating diagnostic and combined therapeutic functions, this new type of ER-targeted PTX-loaded comblike polymer PAsp-*g*-(PEG-ICG) micelle offers a promising strategy for enhanced cancer cell ablation.

## Experimental

### Synthesis of PSI and alkynyl modified PSI

Polysuccinimide (PSI) was synthesized by microwave assisted L-aspartic acid condensation. The detailed synthesis process and characterization of polysuccinimide (PSI), 2-(2-(prop-2-ynyloxy)ethoxy)ethanamine, alkynyl modified PSI (PSI-*g*-alkynyl), azido modified indocyanine green and azido modified polyethylene glycol can be found in the ESI (parts I–IV, Fig. S1–S13†).

### Synthesis of alkynyl modified poly(aspartic acid) (PAsp)

200 mg of PSI-*g*-alkynyl was suspended in water (0.4 ml) and cooled to 0 °C under stirring, 1 M NaOH was added dropwise and the pH of the solution was adjusted to above 10. After hydrolysis for 30 min, 1 M HCl was added dropwise to neutralize the solution, then dialysed against deionized water for 2 days and lyophilized to obtain alkynyl modified PAsp (PAsp-*g*-alkynyl) (Fig. S14†).

### Synthesis of comblike PAsp-*g*-(PEG-ICG) polymers

100 mg of PAsp-*g*-alkynyl (~0.5 mmol) was added into a round-bottom flask (5 ml) and dissolved in a mixture of DMF (0.2 ml) and DMSO (0.2 ml). After that, an mPEG-N<sub>3</sub> (200 mg, 0.20 mmol, 40 mol%) DMF (in 0.2 ml) solution, ICG-N<sub>3</sub> (83.8 mg, 0.125 mmol, 25 mol%) and CuI (3.10 mg, 16.2 µmol) were added into the above solution. The flask was sealed and evacuated, and then refilled with nitrogen; this process was repeated three times to remove traces of oxygen; *N,N,N',N',N''*-

pentamethyldiethylenetriamine (PMDETA, 6.80  $\mu\text{L}$ , 32.5  $\mu\text{mol}$ ) was dissolved in degassed DMSO (0.20 ml) and added into the flask by using an injection syringe. The reaction mixture was stirred at 35  $^{\circ}\text{C}$  for 24 h. After the reaction was complete, the reaction solution was precipitated by adding excess ether, the precipitate was isolated by centrifugation, the resulting crude product was redissolved in DCM and precipitated in ether several times, and then the product was redissolved in water, and dialysed against EDTA solution to remove copper, and then against deionized water, followed by lyophilization. Finally, comblike PAsp-*g*-(PEG-ICG) was obtained as a fluffy solid (Fig. S15 $\dagger$ ).

### Synthesis of alkynyl modified PLys

641 mg of poly- $\epsilon$ -lysine (PLys) (5.00 mmol) was dissolved in methanol (20 ml), and then 3-bromo-1-propyne (298 mg, 2.5 mmol, 0.5 equiv.) and DIPEA (808 mg, 6.25 mmol, 2.5 equiv.) were added into the above solution. The reaction mixture was stirred at 50  $^{\circ}\text{C}$  for 24 h. After the reaction was complete, the reaction mixture was concentrated under vacuum and then precipitated using ether. The resulting solid was redissolved in methanol and reprecipitated by adding excess ether, this process was repeated three times, and then the product was dried under vacuum to obtain alkynyl modified PLys (PLys-*g*-alkynyl, 629.3 mg).

### Synthesis of comblike PLys-*g*-(PEG-ICG) polymers

168 mg of PLys-*g*-alkynyl ( $\sim 1.0$  mmol) was added into a round-bottom flask (5 ml) and dissolved in DMSO (1 ml), mPEG- $\text{N}_3$  (300 mg, 0.30 mmol, 30 mol%), ICG- $\text{N}_3$  (67 mg, 0.1 mmol) and CuI (3.8 mg, 20  $\mu\text{mol}$ ) were then added into the above flask. The flask was sealed and evacuated, and then refilled with nitrogen; this process was repeated three times to remove traces of oxygen, and then PMDETA (8.4  $\mu\text{L}$ , 40  $\mu\text{mol}$ ) was added into the flask under nitrogen. The reaction mixture was stirred at 50  $^{\circ}\text{C}$  for 24 h. After the reaction was complete, the resulting solution was precipitated by adding excess ether, the precipitate was isolated by centrifugation, and the resulting crude product was redissolved in methanol and precipitated in ether three times, and then the product was redissolved in water, and dialysed against deionized water, followed by lyophilization. PLys-*g*-(PEG-ICG) was obtained as a fluffy green solid (398 mg). Note: ICG is not stable in the presence of amine, thus PLys-*g*-(PEG-ICG) should be freshly prepared and used.

### Drug loading content and encapsulation efficiency of PTX@PAsp-*g*-(PEG-ICG) micelles

Different amounts of PTX ethanol solution (30 mg  $\text{ml}^{-1}$ ) were added into PAsp-*g*-(PEG-ICG) aqueous solution (10 mg  $\text{ml}^{-1}$ ) under stirring, and the obtained PTX@PAsp-*g*-(PEG-ICG) micelles were centrifuged at 5000*g* for 5 min to remove unloaded PTX and the supernatant was obtained as a PTX@PAsp-*g*-(PEG-ICG) micelle solution.

To determine the drug loading capacity (DLC) and encapsulation efficiency (EE), PTX@PAsp-*g*-(PEG-ICG) micelle solution

(100  $\mu\text{L}$ ) was diluted to a constant volume (10.00 ml) using acetonitrile. The PTX concentration of the diluted solution was determined by HPLC using a standard PTX curve (Fig. S18 $\dagger$ ). The as-prepared PTX@PAsp-*g*-(PEG-ICG) micelles could be easily sterilized by passing through 0.22  $\mu\text{m}$  filters, which is applicable in clinical studies:

$$\text{DLC (\%)} = W_{\text{PTX}} / (W_{\text{P}} + W_{\text{PTX}}) \times 100\%$$

$$\text{EE (\%)} = W_{\text{PTX}} / W_{\text{T}} \times 100\%$$

where  $W_{\text{PTX}}$  refers to the weight of PTX in the supernatant,  $W_{\text{P}}$  refers to the weight of PAsp-*g*-(PEG-ICG), and  $W_{\text{T}}$  is the weight of the total added PTX.

### Stability of PTX@PAsp-*g*-(PEG-ICG) micelles

To investigate the stability of PTX@PAsp-*g*-(PEG-ICG) micelles, we stored the PTX@PAsp-*g*-(PEG-ICG) micelle solution at room temperature or at 4  $^{\circ}\text{C}$ , and it was stable at least for one week at room temperature and for three months at 4  $^{\circ}\text{C}$  without precipitation.

### Characterization of PTX@PAsp-*g*-(PEG-ICG) micelles

For determining the morphology and size of PTX@PAsp-*g*-(PEG-ICG) micelles, transmission electron microscopy (TEM) images were obtained on a Tecnai G2 20 TWIN (FEI, America), TEM at an accelerating voltage of 200 kV. For sample preparation, a 50  $\mu\text{g ml}^{-1}$  micelle solution was added dropwise onto a carbon-coated copper grid and air dried, and then observed by TEM (Fig. S17 $\dagger$ ).

Absorption spectra of ICG- $\text{N}_3$  and PAsp-*g*-(PEG-ICG) were recorded using a Lambda 750 (PerkinElmer, America) ultraviolet-visible spectrophotometer (Fig. S19 $\dagger$ ). The absorption spectra revealed that the maximal absorption peak and peak pattern remained nearly the same, indicating the integrity of ICG after the modification process.

The standard curve of ICG- $\text{N}_3$  in DMSO (792 nm) was measured by using UV-vis spectroscopy (Fig. S20 $\dagger$ ). To measure the content of ICG in PAsp-*g*-(PEG-ICG), PAsp-*g*-(PEG-ICG) was dissolved in DMSO at a concentration of 19.50  $\mu\text{g ml}^{-1}$ ; the absorption value was measured as 0.7356, based on the ICG- $\text{N}_3$  standard curve (Fig. S20 $\dagger$ ), and the content of ICG in PAsp-*g*-(PEG-ICG) was calculated as 14.1 wt%.

### Cell culture

U-87 MG cells were cultured in MEM medium supplemented with 10% fetal bovine serum (FBS) with 100 U  $\text{ml}^{-1}$  penicillin and 0.1 mg  $\text{ml}^{-1}$  streptomycin at 37  $^{\circ}\text{C}$  in a humidified 5%  $\text{CO}_2$  incubator (HERAcell 150i). For SK-OV-3 cells, MEM medium was changed to McCoy's 5A medium.

Subculture was performed every two days. For general cell culture, a 25  $\text{cm}^2$  cell culture flask was used. Briefly, cells were digested using 0.25% trypsin (1 ml) containing 0.02% EDTA solution at 37  $^{\circ}\text{C}$  for 3 min (U-87 MG and HepG2 cells) or 5 min (SK-OV-3 cells), and then complete cell culture medium (2 ml) was added and the cells were gently piped off at the

bottom of the culture flask. The cell suspension was centrifuged at 100g for 3 min, the supernatant was discarded, complete culture medium (3 ml) was added and gently shaken to obtain a cell suspension. The cell suspension (1 ml) was transferred to a new 25 cm<sup>2</sup> cell culture flask and the complete culture medium (4 ml) was added and resuspended, and then placed in a CO<sub>2</sub> cell incubator for further culture.

#### Cellular uptake of PTX@PAsp-g-(PEG-ICG) micelles

U-87 MG cells were seeded in 6-well plates at a density of  $5 \times 10^5$  cells per well. After incubation for 24 h, the culture medium was discarded, and PTX@PAsp-g-(PEG-ICG) micelles in culture medium were added (PTX at  $1 \mu\text{g ml}^{-1}$ , PAsp-g-(PEG-ICG) at  $2.54 \mu\text{g ml}^{-1}$ , DLC = 28.2%). At different time intervals, the U-87 MG cells were digested, centrifuged and resuspended in PBS and analyzed by FCM. The excitation wavelength was 638 nm, and a 755 nm long pass emission filter was used for detecting the fluorescence intensity of ICG in U-87 MG cells.

#### Uptake mechanism of PTX@PAsp-g-(PEG-ICG)

SK-OV-3 cells were seeded in 6-well plates at a density of 500 000 cells per well. After 24 h of incubation, the culture medium was discarded, and the cells were pretreated with PBS (37 °C), PBS (4 °C), 2-deoxy-D-glucose (50 mM)/NaN<sub>3</sub> (10 mM) and sucrose (0.45 M) for 30 minutes, respectively. Then supernatants were discarded, and PTX@PAsp-g-(PEG-ICG) (PTX  $20 \mu\text{g ml}^{-1}$ , DL ~ 30%) (2 ml) dispersed in PBS was added, and incubated for a further 2 h. After that cells were digested, centrifuged and resuspended in PBS and analyzed by flow cytometry. The excitation wavelength was 638 nm, and a 755 nm long pass emission filter was used.

Low temperature incubation: PBS (4 °C); ATP depletion study (for energy depletion of cells): 2-deoxy-D-glucose (50 mM)/NaN<sub>3</sub> (10 mM); hypertonic study (for inhibition of clathrin mediated endocytosis): sucrose (0.45 M).

#### ROS detection

SK-OV-3 cells were seeded in a 35 mm coverglass bottom dish at  $5 \times 10^4$  cells per well. After 24 h of incubation, PTX@PAsp-g-(PEG-ICG) micelles (PTX at  $1 \mu\text{g ml}^{-1}$ , PAsp-g-(PEG-ICG) at  $2.54 \mu\text{g ml}^{-1}$ , DLC = 28.2%) in cell culture medium (2 ml) were added; the untreated group was used as the control. After incubation for one hour, the culture medium was discarded, and 2',7'-dichlorofluorescein diacetate (DCFH-DA, 10 μM) and Hoechst 33342 ( $10 \mu\text{g ml}^{-1}$ ) in serum free medium (1 ml) were added and incubated for a further 0.5 h. After the ROS indicator DCFH-DA was loaded into cells, the supernatant was discarded, cells were washed with PBS to remove excess DCFH-DA, and then PBS (1 ml) was added to maintain a suitable osmotic pressure. The laser+ group was then irradiated with a 785 nm laser for 30 s. All groups were observed by CLSM (Olympus FV1000) immediately, and images were analyzed.

In the DCFH-DA loading process, membrane-permeable DCFH-DA (non-fluorescent) was hydrolyzed into membrane-

impermeable DCFH (non-fluorescent) by esterase in cells, and ROS could oxidize DCFH (non-fluorescent) into fluorescent DCF (Ex = 480 nm, Em = 525 nm), thus different concentrations of ROS could be easily detected by determining the green fluorescence change within the cells.

All measurement parameters were as follows: sampling speed: 10.0 μs per pixel; C.A.: 80 μm; objective lens UPLSAPO 60×O NA: 1.35; laser wavelength: 488 nm; laser transmissivity: 5.0%; PMT voltage: 550 V; excitation DM name: DM405/488; emission wavelength: 520 nm.

#### Subcellular distribution of PTX@PAsp-g-(PEG-ICG) micelles and PTX@PLys-g-(PEG-ICG) micelles in cells

U-87 MG and SK-OV-3 cells were seeded in a 35 mm coverglass bottom dish at  $5 \times 10^4$  cells per well. After 24 h of incubation, PTX@PAsp-g-(PEG-ICG) micelles (PTX at  $1 \mu\text{g ml}^{-1}$ , PAsp-g-(PEG-ICG) at  $2.54 \mu\text{g ml}^{-1}$ , DLC = 28.2%) or PTX@PLys-g-(PEG-ICG) micelles were added. After incubation for two hours, the cell culture medium was discarded, washed with PBS three times, and fixed using a 4% neutral paraformaldehyde solution for 10 min. Then cells were washed with PBS three times, Hoechst 33342 ( $10 \mu\text{g ml}^{-1}$ ) and ER tracker green (1 μM) were added (1 ml) and incubated for 20 min at 37 °C, for staining the cell nucleus and ER, respectively. After that, the supernatants were discarded and cells were washed with PBS twice and observed by CLSM. Colocalization of ER and ICG was performed using ImageJ with JACoP plugin, which could be downloaded from <https://imagej.nih.gov/ij/plugins/index.html>.

#### Photothermal effect of PAsp-g-(PEG-ICG) micelles

PAsp-g-(PEG-ICG) micelles were dissolved in PBS (0–100 μg ml<sup>-1</sup>), and a 100 μL polymer micelle solution was added into a 96-well plate and irradiated with a 785 nm laser (2 W cm<sup>-2</sup>); the temperature at different time intervals was determined by using a thermocouple thermometer.

#### Cell apoptosis

U-87 MG cells were seeded in 6-well plates at a density of  $5 \times 10^5$  cells per well. After 24 h of incubation, the culture medium was discarded, PTX@PAsp-g-(PEG-ICG) micelles in 2 ml culture medium were added (PTX at  $1 \mu\text{g ml}^{-1}$ , PAsp-g-(PEG-ICG) at  $2.54 \mu\text{g ml}^{-1}$ , DLC = 28.2%), and clinically applied Taxol® was used as a comparison. The concentration of PTX was  $1 \mu\text{g ml}^{-1}$ . After incubation for 12 h, the L+ group was irradiated with a 785 nm laser (0.2 W cm<sup>-2</sup>, 5 min), and further incubated for 12 h. After that, the cell morphology was observed by contrast microscopy, then the cells were digested with EDTA free trypsin for 3 minutes, a complete cell culture medium was added, and the cell suspension was centrifuged at 800 rpm for 3 minutes. Then the cells were washed with PBS and the supernatant was removed. 100 μl of annexin V binding solution was added. 5 μl annexin V-FITC and 5 μl propidium iodide (PI) solution were added to the cell suspension. Then the cell suspension was incubated for 15 minutes with protection from light and 400 μl annexin V binding solution was

added. Cell apoptosis was analyzed by flow cytometry (Gallios, Beckman Coulter). Untreated cells stained with annexin V-FITC and PI were used as a negative control. The excitation and filter were as follows: for annexin V, Ex = 488 nm, Em = 525 BP; for PI, Ex = 488 nm, Em = 620 BP. At the early stage of cell apoptosis, phosphatidylserine in the inner layer of the cell membrane would flip to the outer surface of the cell, which could bind specifically to annexin V-FITC, but the cell membrane was still intact and PI could not pass through, thus early stage cell apoptosis would be observed on staining with annexin V-FITC (+) and PI (-). At the late stage of cell apoptosis, the cell membrane was disrupted and PI could pass through the cell membrane and bind to the cell nucleus, and therefore cell apoptosis at the late stage would be observed on staining with annexin V-FITC (+) and PI (+).<sup>25,26</sup>

### Cell viability

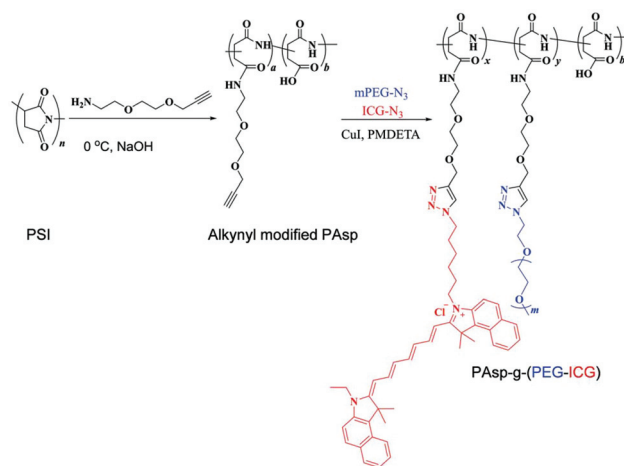
U-87 MG cells were seeded in 96-well plates at a density of 5000 cells per well; the volume of culture medium was all fixed to 100  $\mu$ L. After incubation for 24 h, the culture medium was replaced with a culture containing pharmaceuticals, and incubated for 24 h, the laser+ group was irradiated with a 785 nm laser for 5 min. At 48 h and 72 h, the cell viability was determined by CCK8 assay.

### Biodistribution of PTX@PAsp-g-(PEG-ICG) micelles in U-87 MG bearing mice

All surgical procedures and post-operation animal care were conducted according to the guidelines of the Council for the Purpose of Control and Supervision of Experiments on Animals, the Ministry of Health, and the government of China. All the animal experimental procedures were approved by the Institutional Animal Care and Use Committee of the Fudan University, Shanghai, China. Female Balb/c nude mice of 5 weeks old were obtained from the Shanghai SLAC Laboratory Animal Center (Shanghai, China) and maintained on a 12–12 h light–dark cycle in independent ventilated cages. All mice were kept for one more week before experiments.

To obtain the xenograft of human glioma tumors in the nude mice, U-87 MG cells were suspended at  $3 \times 10^7$  cells per ml in FBS free culture medium. A total of  $3 \times 10^6$  cells in 100  $\mu$ L culture medium suspension was injected subcutaneously into the dorsal site of the right foreleg of each 6-week old nude mouse.

PAsp-g-(PEG-ICG) and PTX@PAsp-g-(PEG-ICG) micelles were intravenously administered through the tail vein of U-87 MG bearing mice at a PTX dosage of 10 mg kg<sup>-1</sup>. At different time intervals, the mice were anaesthetized by isoflurane inhalation, and the fluorescence of ICG was visualized by using a small animal imaging system (*In Vivo Xtreme*, Bruker), the excitation filter was 760 nm with a bandwidth of 30 nm, and the emission filter was 830 nm with a bandwidth of 30 nm, and the acquisition time was fixed to 2 s.



**Scheme 1** The detailed preparation procedure of the comblike PAsp-g-(PEG-ICG) polymers.

## Results and discussion

On the basis of rational design, 2-(2-(prop-2-ynoxy)ethoxy)ethanamine, mPEG-N<sub>3</sub> and ICG-N<sub>3</sub> were employed to synthesize PAsp-g-(PEG-ICG). First, the alkyne-modified PAsp was prepared by reacting 2-(2-(prop-2-ynoxy)ethoxy)ethanamine with PSI at ambient temperature (ESI, parts I, II and III, Fig. S1–14<sup>†</sup>). Then, the comblike PAsp-g-(PEG-ICG) was prepared by grafting mPEG-N<sub>3</sub> and ICG-N<sub>3</sub> onto alkyne-modified PAsp with CuAAC as a catalyst (Scheme 1 and Fig. S15<sup>†</sup>).

The molecular weight of the PAsp-g-(PEG-ICG) was evaluated (Fig. S16<sup>†</sup>) with a number-average molecular weight of  $2.5 \times 10^4$ , whereas the number-average molecular weight of alkyne-modified PAsp was  $1.3 \times 10^4$ , indicating the successful grafting. The as-prepared PAsp-g-(PEG-ICG) was highly dispersible in water. PAsp-g-(PEG-ICG) dispersed in water resulted in over 99% decrease in its fluorescence intensity in comparison with its performance in DMSO solution, presumably due to the aggregation of the hydrophobic ICG groups in the aqueous solution, which resulted in the formation of polymeric micelles (Fig. 1B). In this regard, given that anti-cancer drugs usually bear aromatic and hydrophobic molecules, paclitaxel (PTX) was selected to tailor the drug loading performance of PAsp-g-(PEG-ICG). The formation procedure of drug-encapsulated polymeric micelles (PTX@PAsp-g-(PEG-ICG)) is shown in Fig. 1A. The drug loading content of PTX@PAsp-g-(PEG-ICG) was 28 wt% with an encapsulation efficiency of up to 95% (Table S1 and Fig. S17<sup>†</sup>). PTX could be solubilized up to 2 mg mL<sup>-1</sup> in aqueous solution with good stability over one week at room temperature, presumably due to the strong aromatic and hydrophobic interactions between ICG and PTX. The formation of PTX@PAsp-g-(PEG-ICG) micelles was confirmed by TEM analysis (Fig. 1C and Fig. S18<sup>†</sup>) with a hydrodynamic size of  $45 \pm 11$  nm (Fig. 1D). It is noteworthy that nanomedicine with sizes of around 50 nm can take full advantage of the EPR effect for an optimal cell-uptake effect,<sup>27,28</sup> thereby the desired size of PTX@PAsp-g-(PEG-ICG) micelles may be beneficial for

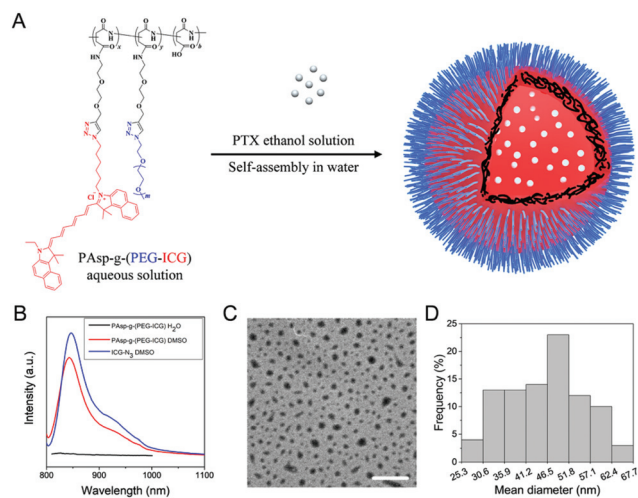


**Fig. 1** Preparation and characterization of the PAsp-*g*-(PEG-ICG) micelles. (A) Scheme for preparation of PTX loaded micelles. PAsp-*g*-(PEG-ICG) micelles were formed by directly adding PTX ethanol solution into PAsp-*g*-(PEG-ICG) aqueous solution. (B) Fluorescence properties of PAsp-*g*-(PEG-ICG) micelles in water (dark line) and DMSO (red line) compared with ICG-N<sub>3</sub> in DMSO (blue line) (Ex = 768 nm, the concentration of PAsp-*g*-(PEG-ICG) in both water and DMSO were 50 μg mL<sup>-1</sup>). Decrease of fluorescence of PAsp-*g*-(PEG-ICG) in water indicating the aggregation of ICG and the formation of micelles. (C) TEM image of PTX@PAsp-*g*-(PEG-ICG) micelles (DLC = 28%) (scale bar is 500 nm). (D) Statistical data of PAsp-*g*-(PEG-ICG) micelles' diameter in (C), 100 polymeric micelles were measured.

their intra-tissue and intracellular delivery as well as retention for desired subcellular ER-targeted drug delivery.

To study the ER-targeted delivery ability of PTX@PAsp-*g*-(PEG-ICG) micelles, we employed two different cancer cell lines (U-87 MG and SK-OV-3) to determine the subcellular distribution of PTX@PAsp-*g*-(PEG-ICG) micelles. Both U-87 MG and SK-OV-3 cells were incubated with PTX@PAsp-*g*-(PEG-ICG) micelles for 2 h. The ER of the U-87 MG and the SK-OV-3 cells was then stained with ER tracker green.

Using confocal laser scanning microscopy, we found that the red fluorescence of ICG overlapped perfectly with the green fluorescence of ER in the U-87 MG cancer cell line (Fig. 2A and Fig. S19A†). The fluorescence intensities of ICG and ER on the yellow cross line in the enlarged picture were quantified as shown in Fig. 2D. The fluorescence intensity curves on the right side indicated ICG (red) and ER (green) in the vertical direction, while the bottom part is the corresponding curves in the horizontal direction. It is clear that the green curve (ER) almost completely overlays the red curve (ICG) with Pearson's coefficient  $r = 0.96$ , indicating high colocalization of PTX@PAsp-*g*-(PEG-ICG) micelles and ER<sup>29</sup> to confirm the intended ER targeting of PAsp-*g*-(PEG-ICG) micelles. Meanwhile, the results obtained from SK-OV-3 cell lines with Pearson's coefficient  $r = 0.93$  were in good agreement with the results above (Fig. 2B, E and Fig. S19B†), also demonstrating

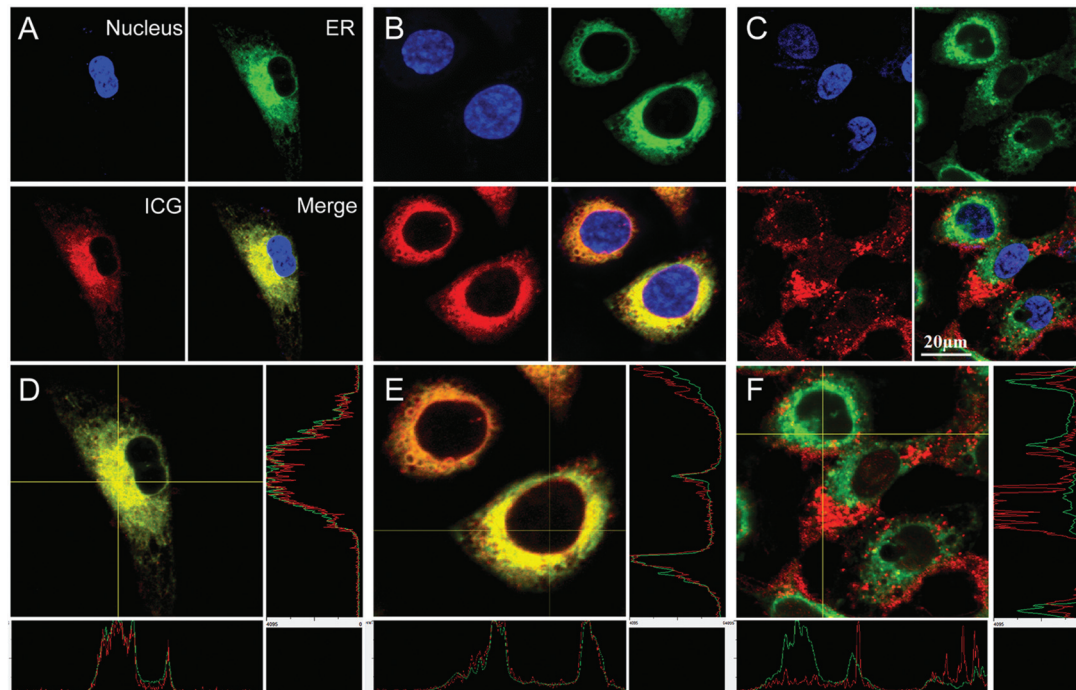
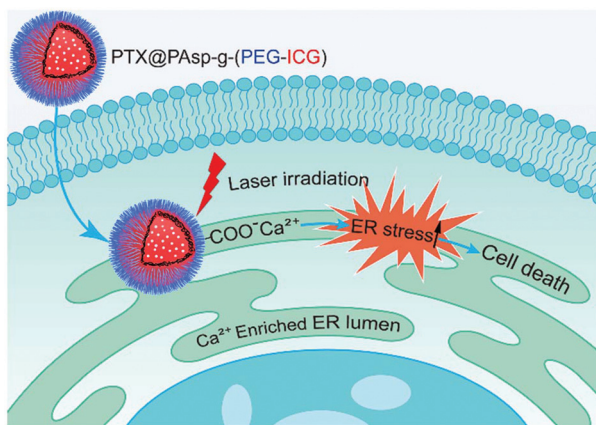


**Fig. 2** Subcellular distribution of PTX@PAsp-*g*-(PEG-ICG) and PTX@PLys-*g*-(PEG-ICG) micelles. (A) The distribution of PTX@PAsp-*g*-(PEG-ICG) micelles in U-87 MG cells. (B) The distribution of PTX@PAsp-*g*-(PEG-ICG) micelles in SK-OV-3 cells. (C) The distribution of PTX@PLys-*g*-(PEG-ICG) micelles in U-87 MG cells. (D) Quantified fluorescence cross-section distribution of ICG (red curve) and ER marker (green curve) in U-87 MG cells after treatment with PTX@PAsp-*g*-(PEG-ICG). (E) Quantified fluorescence cross-section distribution of ICG (red curve) and ER marker (green curve) in SK-OV-3 cells after treatment with PTX@PAsp-*g*-(PEG-ICG). (F) Quantified fluorescence cross-section distribution of ICG (red curve) and ER marker (green curve) in U-87 MG cells after treatment with PTX@PLys-*g*-(PEG-ICG).



**Scheme 2** Illustration of the PTX@PAsp-g-(PEG-ICG) ER targeting process and mechanism of cell death. PTX@PAsp-g-(PEG-ICG) micelles accumulate in the ER lumen through coordination affinity of the Ca(II) ions to the carboxyl groups of PAsp. Upon laser irradiation of the photosensitizer ICG, the generated ROS would lead to elevated ER stress and induce cancer cell death.

high colocalization of PTX@PAsp-g-(PEG-ICG) micelles and ER in SK-OV-3 cells.

We also investigated the cell uptake mechanism of PTX@PAsp-g-(PEG-ICG). The fluorescence intensity of SK-OV-3 cells was reduced to 33% at 4 °C temperature compared to the incubation at 37 °C. Meanwhile, the ATP depletion treatment and hypertonic treatment cannot inhibit the cell uptake of PTX@PAsp-g-(PEG-ICG) (Fig. S27<sup>†</sup>). Thus, the cell uptake mechanism of PTX@PAsp-g-(PEG-ICG) was not through endocytosis (ATP required), but largely attributed to passive transportation.

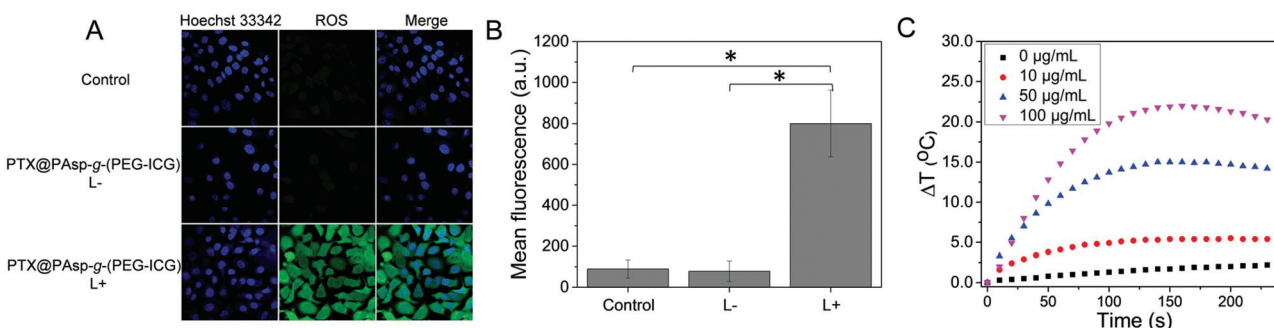
To evaluate the importance of the carboxyl groups in PAsp for the intended ER targeting, we prepared a control group by replacing PAsp with amino containing poly-ε-lysine (PLys) in the copolymer. The resulting PLys-g-(PEG-ICG) micelles displayed a subcellular distribution substantially different from that of PTX@PAsp-g-(PEG-ICG) micelles (Fig. 2C, F and Fig. S19C<sup>†</sup>). The red and green curves regarding ICG and ER in

Fig. 2F have poor correlation with Pearson's coefficient  $r = 0.354$ , indicating the weak interaction between PLys-g-(PEG-ICG) and ER. All the above evidence revealed the most likely coordination effect between the carboxyl group of the PAsp and the high concentration of Ca(II) ions in the ER lumen, which mediated the ER-targeting effect by PAsp-g-(PEG-ICG) micelles, where the possible mechanism is illustrated in Scheme 2.

We then showed that the fluorescence performance of PTX@PAsp-g-(PEG-ICG) micelles in U-87 MG cells reached the highest fluorescence intensity after 8 h incubation, indicating the fast accumulation of PTX@PAsp-g-(PEG-ICG) micelles in U-87 MG cells (Fig. S22–S24<sup>†</sup>). Thus, when the accumulation of PTX@PAsp-g-(PEG-ICG) micelles reaches a therapeutic concentration in the ER lumen, we could take the advantages of both PDT and PTT effects from ICG to disrupt oncogenic proteins or survival factors within the ER of cancer cells. To demonstrate the PDT and PTT effects of PTX@PAsp-g-(PEG-ICG) micelles, SK-OV-3 cells were incubated with PTX@PAsp-g-(PEG-ICG) micelles. Compared with the control group and the PTX@PAsp-g-(PEG-ICG) group without laser irradiation (nearly no green fluorescence), we found that only when both PTX@PAsp-g-(PEG-ICG) micelles and laser irradiation were applied to SK-OV-3 cells, 10-fold ROS were generated (Fig. 3A and B), indicating the great potential of the PDT effect from PTX@PAsp-g-(PEG-ICG) micelles.

It is well known that the ER in cancer cells is overloaded with synthesized proteins due to malignant proliferation, and further gives rise to ER stress.<sup>30</sup> In order to survive this stressful environment, cancer cells have evolved an unfolded protein response (UPR) to relieve ER stress compared to normal cells.<sup>31–33</sup> Thus we could tip the balance of the ER environment towards cancer cell death by an overwhelming ER stress, while the normal cells without light irradiation or PAsp-g-(PEG-ICG) would stay intact.

Furthermore, the PTT effect of PAsp-g-(PEG-ICG) micelles was also evaluated by measuring temperature elevation at different concentrations under laser irradiation. We found that the temperature of the solution was increased by nearly 15 °C



**Fig. 3** ROS generation and the PTT effect of PTX@PAsp-g-(PEG-ICG) micelles. (A) Detection of intracellular ROS by incubating DCFH-DA with PTX@PAsp-g-(PEG-ICG) treated SK-OV-3 cells with/without laser irradiation ( $0.2 \text{ W cm}^{-2}$ , 785 nm, 30 s). (B) Quantification of ROS generation based on fluorescence in (A), the mean fluorescence of 15–20 cells was measured,  $*p < 0.001$ . (C) The temperature elevation curves of different concentrations of PAsp-g-(PEG-ICG) micelles under 785 nm laser irradiation ( $2 \text{ W cm}^{-2}$ ).

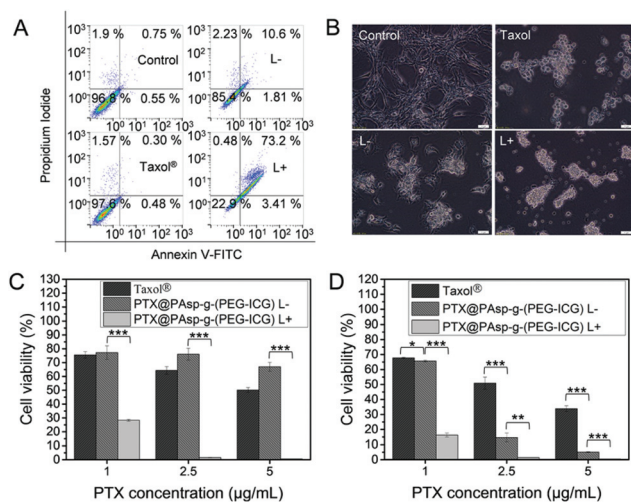


**Fig. 4** *In vitro* evaluation of PTX@PAsp-g-(PEG-ICG) micelles. (A) Flow cytometric analysis of apoptosis of U-87 MG cells induced by Taxol® and PTX@PAsp-g-(PEG-ICG) micelles with/without laser irradiation ( $0.2 \text{ W cm}^{-2}$ ,  $785 \text{ nm}$ ,  $5 \text{ min}$ ). (B) The morphology of U-87 MG cells incubated with culture medium, Taxol® and PTX@PAsp-g-(PEG-ICG) micelles with/without laser irradiation ( $0.2 \text{ W cm}^{-2}$ ,  $785 \text{ nm}$ ,  $5 \text{ min}$ ). Cell viability of U-87 MG cells at (C) 48 h and (D) 72 h incubated with Taxol and PTX@PAsp-g-(PEG-ICG) micelles with/without laser irradiation ( $2 \text{ W cm}^{-2}$ ,  $785 \text{ nm}$ ,  $30 \text{ s}$ ). \* $p < 0.05$ , \*\* $p < 0.01$ , \*\*\* $p < 0.001$ .

within 130 s at the PAsp-g-(PEG-ICG) micelle concentration of  $50 \mu\text{g mL}^{-1}$ , whereas the temperature increased by only  $1.6 \text{ }^\circ\text{C}$  in the absence of PAsp-g-(PEG-ICG) micelles (Fig. 3C). As previously reported, temperature elevation above  $43 \text{ }^\circ\text{C}$  would result in irreversible protein denaturation and disruption of the cellular membrane,<sup>34</sup> hence the accumulated PTX@PAsp-g-(PEG-ICG) micelles in the ER were able to further give rise to ER stress in combination with PDT and exhibit a synergistic effect on cancer cell killing.

After demonstrating that PTX@PAsp-g-(PEG-ICG) micelles could target the ER of cancer cells and generate ROS and

hyperthermia under laser irradiation, we went on to investigate if these effects could cause sufficient damage to proteins within the ER and lead to the apoptosis of cancer cells. U-87 MG cells treated with Taxol® showed negligible cell apoptosis compared with the control group, whereas cells incubated with PTX@PAsp-g-(PEG-ICG) micelles without laser irradiation showed 10.6% of cell apoptosis at the late stage (Fig. 4A). When laser irradiation ( $0.2 \text{ W cm}^{-2}$ ,  $785 \text{ nm}$ ,  $5 \text{ min}$ ) was applied, remarkable cell apoptosis (73.2%) at the late stage was observed. Since the treatment at this concentration of PTX@PAsp-g-(PEG-ICG) micelles under  $0.2 \text{ W cm}^{-2}$  of laser irradiation could not induce prominent temperature elevation, it is largely attributed that the cell apoptosis was induced by ROS generation through enhanced ER stress.

To evaluate the PDT effect of ER-targeting PTX@PAsp-g-(PEG-ICG) micelles, we conducted *in vitro* studies in U-87 MG cell lines. The morphology of the cells at the PTX concentration of  $1 \mu\text{g mL}^{-1}$  is shown in Fig. 4B. Cell contraction was observed immediately after laser irradiation of PTX@PAsp-g-(PEG-ICG) micelles (Fig. 4B) or PAsp-g-(PEG-ICG) micelles (Fig. S25†), while all the treatment without laser irradiation showed negligible cell contraction, implying the effective PDT arising from PAsp-g-(PEG-ICG) or PTX@PAsp-g-(PEG-ICG) micelles. The cell viability of U-87 MG cells at different PTX concentrations was measured by Cell Counting Kit-8 (CCK-8) assay (Fig. 4C and D). With the increasing concentrations of PTX and PAsp-g-(PEG-ICG), the viability of U-87 MG cells decreased after 48 h or 72 h incubation. When laser irradiation was applied, U-87 MG cells could hardly survive at PTX concentrations of 2.5 and  $5 \mu\text{g mL}^{-1}$  (corresponding to ICG 0.9 and  $1.8 \mu\text{g mL}^{-1}$ , respectively), indicating that ER stress induced cancer cell apoptosis could greatly improve the chemotherapy. Moreover, it is noteworthy that the good chemotherapeutic effect of PTX enables it to play a key role in killing U-87 MG cells after 72 h incubation with PTX@PAsp-g-(PEG-ICG) micelles, compared to the negligible cytotoxicity at the same concentration of PAsp-g-(PEG-ICG) (data not shown).

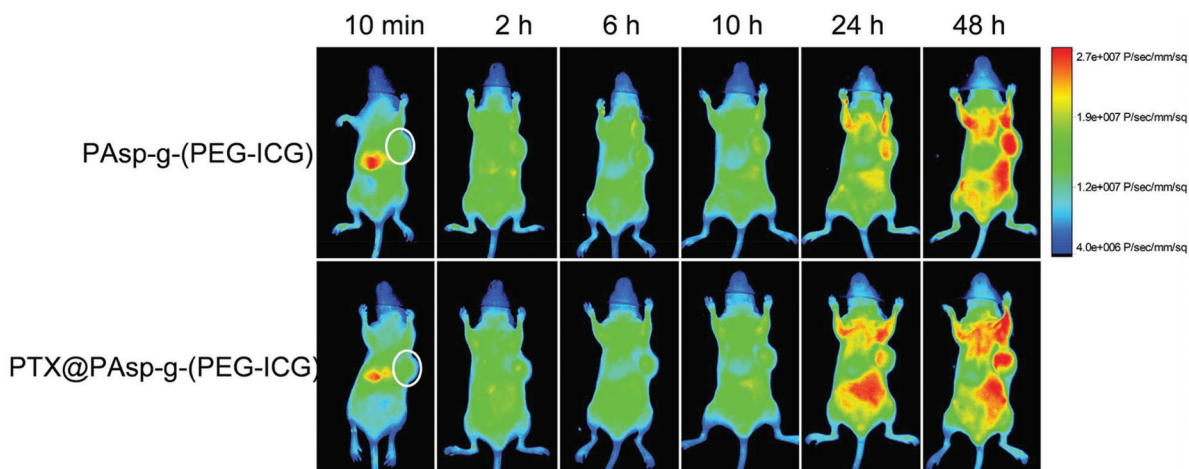


**Fig. 5** *In vivo* biodistribution images of PAsp-g-(PEG-ICG) and PTX@PAsp-g-(PEG-ICG) micelles in U-87 MG tumor-bearing mice after intravenous injection at different time intervals. (Ex =  $760 \text{ nm}$ , Em =  $830 \text{ nm}$ , exposure time =  $2 \text{ s}$ ). The white circles are the position of the tumors.

We further evaluated the accumulation effect on the *in vivo* biodistribution of PTX@PAsp-*g*-(PEG-ICG) micelles in U-87 MG tumor-bearing nude mice. PAsp-*g*-(PEG-ICG) and PTX@PAsp-*g*-(PEG-ICG) (PTX 10 mg kg<sup>-1</sup>, 0.1 mL) micelles were administered into U-87 MG tumor-bearing mice intravenously. The distribution of PAsp-*g*-(PEG-ICG) micelles and PTX@PAsp-*g*-(PEG-ICG) micelles can be identified after injection (Fig. 5), substantiating the minimum effect of PTX on the distribution of micelles. Compared with free ICG groups, both micelles exhibited an enhanced retention time with no obvious decrease of fluorescence intensity after 48 h post administration, which was attributed to the grafted PEG chains that was beneficial for prolonging the circulation time (Fig. S28†). PAsp-*g*-(PEG-ICG) and PTX@PAsp-*g*-(PEG-ICG) micelles both displayed high levels of preferential accumulation in the tumor sites driven by the enhanced permeation and retention (EPR) effect.

To demonstrate the anti-cancer effect of PTX@PAsp-*g*-(PEG-ICG) micelles *in vivo*, PTX@PAsp-*g*-(PEG-ICG) micelles (1 mg mL<sup>-1</sup>, 10 mg kg<sup>-1</sup>) were administered intravenously into U-87 MG tumor bearing mice (*n* = 5) at day 0, with Taxol® as a control group. The mice treated with PTX@PAsp-*g*-(PEG-ICG) micelles with laser irradiation were anaesthetized and irradiated using a 785 nm laser with an energy density of 2 W cm<sup>-2</sup> for 5 minutes at 24 h post-injection. After day 21 injection, the tumor volume of the PBS control mice reached the pre-set end points, compared with the mice administered with Taxol® (\*\**p* < 0.01) and PTX@PAsp-*g*-(PEG-ICG) micelles without laser irradiation (\**p* < 0.05) (Fig. S29A†). The Taxol® group outperformed the PTX@PAsp-*g*-(PEG-ICG) micelle group without laser irradiation. The PTX@PAsp-*g*-(PEG-ICG) micelle treated with laser irradiation displayed more effective inhibition with complete tumor remission in two mice at day 21, showing the highest therapeutic efficacy among all the experimental groups. In addition, no significant body weight loss was observed during the course of the study (Fig. S29B†), indicating minimal side effects.

## Conclusions

In summary, we successfully synthesized ER-targeted PAsp-*g*-(PEG-ICG) polymeric micelles with the near-infrared photosensitizer ICG. After loading the anticancer drug PTX, the PTX@PAsp-*g*-(PEG-ICG) micelles were formed to conduct the cell uptake experiments, where the experimental results showed that the polymeric micelles could selectively accumulate in the ER region of cancer cells. Compared with the control group and PTX@PAsp-*g*-(PEG-ICG) group without laser irradiation, 10-fold ROS were generated in the presence of PTX@PAsp-*g*-(PEG-ICG) and laser irradiation, which led to PDT induced ER stress mediated cell apoptosis. Cell viability experiments revealed that the PDT induced ER stress could greatly enhance the therapeutic effect of PTX. PTX@PAsp-*g*-(PEG-ICG) micelles showed ideal distribution and accumulation in the tumor sites of the U-87 MG bearing mice, provid-

ing great promise for manipulating nanomedicine design to achieve the desired ER-targeted delivery both *in vitro* and *in vivo* for targeted synergistic cancer therapy.

## Conflicts of interest

There are no conflicts to declare.

## Acknowledgements

This work was financially supported by the National Natural Science Foundation of China (Grant no. 51633001, 51721002, and 21474017) and the National Key R&D Program of China (Grant no. 2016YFC1100300).

## References

- 1 M. X. Sliwowski and I. Mellman, *Science*, 2013, **341**, 1192–1198.
- 2 B. Vogelstein and K. W. Kinzler, *Nat. Med.*, 2004, **10**, 789–799.
- 3 D. B. Cox, R. J. Platt and F. Zhang, *Nat. Med.*, 2015, **21**, 121–131.
- 4 J. A. Doudna and E. Charpentier, *Science*, 2014, **346**, 1258096.
- 5 L. Li, L. Song, X. Liu, X. Yang, X. Li, T. He, N. Wang, S. Yang, C. Yu, T. Yin, Y. Wen, Z. He, X. Wei, W. Su, Q. Wu, S. Yao, C. Gong and Y. Wei, *ACS Nano*, 2017, **11**, 95–111.
- 6 R. Mout, M. Ray, G. Yesilbag Tonga, Y. W. Lee, T. Tay, K. Sasaki and V. M. Rotello, *ACS Nano*, 2017, **11**, 2452–2458.
- 7 S. Orrenius, B. Zhivotovsky and P. Nicotera, *Nat. Rev. Mol. Cell Biol.*, 2003, **4**, 552–565.
- 8 J. Chen, L. Xu, J. Han, M. Su and Q. Wu, *Desalination*, 2015, **358**, 42–48.
- 9 H. Cabral and K. Kataoka, *J. Controlled Release*, 2014, **190**, 465–476.
- 10 L. Fu, P. Yuan, Z. Ruan, L. Liu, T. Li and L. Yan, *Polym. Chem.*, 2017, **8**, 1028–1038.
- 11 C. H. Wang, W. T. Wang and G. H. Hsiue, *Biomaterials*, 2009, **30**, 3352–3358.
- 12 H. Arimura, Y. Ohya and T. Ouchi, *Biomacromolecules*, 2005, **6**, 720–725.
- 13 M. T. Fatima, A. Chanchal, P. S. Yavvari, S. D. Bhagat, M. Gujrati, R. K. Mishra and A. Srivastava, *Biomacromolecules*, 2016, **17**, 2375–2383.
- 14 N. Liu, B. Li, C. Gong, Y. Liu, Y. Wang and G. Wu, *Colloids Surf., B*, 2015, **136**, 562–569.
- 15 M. Lee, J. Jeong and D. Kim, *Biomacromolecules*, 2015, **16**, 136–144.
- 16 R. Mendichi, A. Giacometti Schieronni, G. Cavallaro, M. Licciardi and G. Giammona, *Polymer*, 2003, **44**, 4871–4879.
- 17 K. Seo and D. Kim, *Acta Biomater.*, 2010, **6**, 2157–2164.

- 18 E. A. Sykes, J. Chen, G. Zheng and W. C. Chan, *ACS Nano*, 2014, **8**, 5696–5706.
- 19 J. Frangioni, *Curr. Opin. Chem. Biol.*, 2003, **7**, 626–634.
- 20 P. Huang, P. Rong, A. Jin, X. Yan, M. G. Zhang, J. Lin, H. Hu, Z. Wang, X. Yue, W. Li, G. Niu, W. Zeng, W. Wang, K. Zhou and X. Chen, *Adv. Mater.*, 2014, **26**, 6401–6408.
- 21 S. W. Ryter, H. P. Kim, A. Hoetzel, J. W. Park, K. Nakahira, X. Wang and A. M. Choi, *Antioxid. Redox Signaling*, 2007, **9**, 49–89.
- 22 A. Szokalska, M. Makowski, D. Nowis, G. M. Wilczynski, M. Kujawa, C. Wojcik, I. Mlynarczuk-Bialy, P. Salwa, J. Bil, S. Janowska, P. Agostinis, T. Verfaillie, M. Bugajski, J. Gietka, T. Issat, E. Glodkowska, P. Mrowka, T. Stoklosa, M. R. Hamblin, P. Mroz, M. Jakobisiak and J. Golab, *Cancer Res.*, 2009, **69**, 4235–4243.
- 23 J. S. Dysart and M. S. Patterson, *Phys. Med. Biol.*, 2005, **50**, 2597–2616.
- 24 P. Agostinis, K. Berg, K. A. Cengel, T. H. Foster, A. W. Girotti, S. O. Gollnick, S. M. Hahn, M. R. Hamblin, A. Juzeniene, D. Kessel, M. Korbelik, J. Moan, P. Mroz, D. Nowis, J. Piette, B. C. Wilson and J. Golab, *Ca-Cancer J. Clin.*, 2011, **61**, 250–281.
- 25 L. Casciola-Rosen, A. Rosen, M. Petri and M. Schlissel, *Proc. Natl. Acad. Sci. U. S. A.*, 1996, **93**, 1624–1629.
- 26 M. van Engeland, F. C. Ramaekers, B. Schutte and C. P. Reutelingsperger, *Cytometry*, 1996, **24**, 131–139.
- 27 L. Tang, X. Yang, Q. Yin, K. Cai, H. Wang, I. Chaudhury, C. Yao, Q. Zhou, M. Kwon, J. A. Hartman, I. T. Dobrucki, L. W. Dobrucki, L. B. Borst, S. Lezmi, W. G. Helferich, A. L. Ferguson, T. M. Fan and J. Cheng, *Proc. Natl. Acad. Sci. U. S. A.*, 2014, **111**, 15344–15349.
- 28 L. Tang, N. P. Gabrielson, F. M. Uckun, T. M. Fan and J. Cheng, *Mol. Pharm.*, 2013, **10**, 883–892.
- 29 S. Bolte and F. P. Cordelieres, *J. Microsc.*, 2006, **224**, 213–232.
- 30 P. Walter and D. Ron, *Science*, 2011, **334**, 1081–1086.
- 31 M. Wang and R. J. Kaufman, *Nature*, 2016, **529**, 326–335.
- 32 M. Wang and R. J. Kaufman, *Nat. Rev. Cancer*, 2014, **14**, 581–597.
- 33 T. Verfaillie, A. D. Garg and P. Agostinis, *Cancer Lett.*, 2013, **332**, 249–264.
- 34 E. B. Dickerson, E. C. Dreaden, X. Huang, I. H. El-Sayed, H. Chu, S. Pushpanketh, J. F. McDonald and M. A. El-Sayed, *Cancer Lett.*, 2008, **269**, 57–66.